University of Baghdad
College of Engineering
JOURNAL OF ENGINEERING

Journal of Engineering
journal homepage: www.jcoeng.edu.iq
Volume 30 Number 11 November 2024

Evaluation of the Effect of Static and Flowing Conditions on the Corrosion Behavior of the Hull of Marine Ships

Abdul-Hamied Ayad Abdul-Hamied *, Abdullah Dhayea Assi

Department of Mechanical Engineering, College of Engineering, University of Baghdad, Baghdad, Iraq

ABSTRACT

Marine ship hulls' corrosion resistance behavior under static and flowing conditions was investigated. The metal of the hull panels of marine ships was chemically and mechanically examined and analyzed, revealing that carbon steel type DIN 1.0501 C35 is employed in constructing the hull of ships in the port of Basrah in Iraq. A corrosion resistance test for this metal was carried out in laboratory-prepared seawater under static and flowing conditions at a flow rate of 1500 liter/hour and various immersion times (12, 24, 48, 120, 168, 336) hours. The temperature was kept constant at 30°C, and a fixed salt concentration of (3.5% sodium chloride). The corrosion rate of C35 carbon steel was calculated using the weight loss method is an effective method for calculating the corrosion rate of carbon steel. The samples were examined using a scanning electron microscope (SEM) for corrosion analysis. Conclusions from this research indicate that an increase in the flow rate resulted in an elevation of the corrosion rate, doubling the corrosion rate compared to samples under static conditions. The corrosion rate exhibited a significant increase during the first 24 hours, followed by a gradual decrease with increasing immersion time. The corrosion rate increased by 682.9%. The speed of corrosion was fast initially, but the weight loss slowed after 24 hours of immersion. A scanning electron microscope (SEM) examination revealed that the flow environment was aggressive for carbon steel. It was much more severe, and the pits and grooves were more significant than the static condition.

Keywords: Ship corrosion, Steel corrosion, Seawater, C35 carbon steel, Weight loss method.

1. INTRODUCTION

Studying corrosion is essential as it is an ongoing challenge faced by the marine industry, especially in ship hulls **(Tamura, 2008)**. Being in direct contact with an aggressive, corrosive environment characterized by exposure to salt water, humidity, and varying flow rates accelerates the deterioration of steel structures through the corrosion process **(Shreir,**

*Corresponding author
Peer review under the responsibility of University of Baghdad.
https://doi.org/10.31026/j.eng.2024.11.06

Article received: 10/01/2024
Article revised: 15/06/2024
Article accepted: 23/06/2024
Article published: 01/11/2024

2013). The corrosive marine environment is one of the challenges facing marine ship hulls due to the corrosion process in seawater **(McCafferty, 2010)**. Corrosion occurs in the hull of marine ships and may be either electrochemical, physical, or biological **(Saravanan and Kumar, 2021)**. Seawater is considered one of the leading causes of the violent corrosion of C35 carbon steel **(Cox and Roetheli, 1931)**. It is considered one of the most widely used materials in various applications and is particularly vulnerable to the corrosive effects of seawater **(Kaouka et al., 2022)**. Seawater can have a very significant impact on the structural integrity of a marine ship and its operational life, as it contains very high salts as well as dissolved oxygen in the water, which are considered essential in accelerating corrosion that leads to local phenomena such as cracks and grooves **(Andrade and Alonso, 1996)**.

The corrosion of marine ships, especially C35 carbon steel, results from a complex electrochemical reaction that is affected by the corrosive nature, such as salty seawater **(Hiekata and Grau, 2015)**. This reaction can cause corrosion of the hulls of marine ships **(Machuca et al., 2014)**. This occurs through the contact of the metal with seawater, contact between two metals, or between the weak and strong areas of the metal itself, where the metal atoms ionize and release electrons into the seawater **(Abd et al., 2022)**. Since salty seawater is considered a conductive electrolyte, it facilitates moving metal atoms from the anode's weak parts to the cathode's more vital areas **(Shakir et al., 2018)**. Iron oxidation reaction can be expressed by losing electrons and producing iron ions that can dissolve in seawater **(Hasan et al., 2016)**. The reaction can be expressed in Eq. (1) below:

$$Fe \rightarrow Fe^{+2} + 2e^{-} \quad (1)$$

Oxygen is reduced as oxygen dissolved in water receives electrons released by iron **(Salman, 2018)**. This reaction is catalyzed by chloride ions present in the saltwater **(Rashid et al., 2017)**. The reaction can be expressed in Eq. (2) below:

$$O_2 + 4H^{+} + 4e^{-} \rightarrow 2H_2O \quad (2)$$

At the same time, the oxygen in the air dissolves in seawater and reacts with water, which is one of the main catalysts for corrosion in addition to moisture **(Muhammad et al., 2021)**. Oxygen with water, moisture, or salty seawater are among the basic materials required in the corrosion process **(Doos and Farhan, 2014)**. Many types of corrosion in the marine environment occur on the hull of marine ships, among which are pitting corrosion, galvanic corrosion, crevice corrosion, microbial corrosion, and stress corrosion cracking **(Ahmed and Makki, 2019)**. The hull of marine ships is made from many materials, In the past, wood was used in hull manufacturing, but designers resorted to steel because of its ease of formation, durability, and resistance to shock **(Majbor et al., 2017)**. On the other hand, steel is not strong enough to resist corrosion, which causes many problems that must be studied and considered **(Alsaadi, 2015)**. Therefore, it is necessary to study the effect of flowing salty sea water on the hulls of marine ships **(Nader and Shather, 2022)**. Many types of steel are used, including carbon steel, high-speed-low alloy steel, and stainless steel **(Dwivedi et al., 2017)**. The most important types of carbon steel used are A36 Steel, C35 Steel, C45 Steel, DH36 Steel, E36 Steel, S235 Steel, and S355 Steel **(Bringas, 2004)**. C35 carbon steel is one of the most common types of carbon steel used in the port of Basra in Iraq.

(Sang and Seung, 2017) They studied the effect of changing seawater flow rate on S355ML steel by evaluating the electrochemical properties of the metal. Flow fields were analyzed in

the seawater environments through particle image velocimetry measurement. The researcher concluded that more significant damage occurred as the flow rate increased due to the effects of corrosion and physical erosion. This increase is due to the more accessible supply of dissolved oxygen, and the reaction rate is enhanced as the flow rate increases. **(Yunze et al., 2020)** studied the corrosion-erosion behavior of X65 carbon steel under different flow conditions and studied the effect of flow on the corrosion rate. Corrosion was tested electrochemically. It was concluded that the surface changed to continuous pits in the corrosion test. Propagation of pits at anodic sites and damage of the corrosion product film at cathodic sites are observed. **(Jiangmin et al., 2021)** Studied the corrosion behavior of structural steel at different flow rates in a seawater environment (from the East China Sea). The corrosion behavior experiments were examined for 30 days, with gradually different seawater flow rates starting from 0, 2, 4, and 6 m/s. The electrochemical method was used to measure the corrosion rate. The results showed that as the flow rate increased, the corrosion reaction increased. The electrochemical corrosion rate increased rapidly in the first days and slowed to a stable situation. Among these results, the flow rate of 2 m/s was the fastest electrochemical corrosion rate. As the flow rate increases, double-layer corrosion products are formed; The outer corrosion products become thinner, and the inner layer of corrosion products gradually forms.

This research aims to evaluate the effect of the flow rate of salty seawater on the corrosion rate of C35 carbon steel **(Sang and Seung, 2017)**. Moreover, the effect of the corrosion process on the surface shape of the samples after the corrosion process is monitored **(Yunze et al., 2020)**. Moreover, the corrosion behaviour during the immersion period was studied using the total immersion method of samples **(Jiangmin et al., 2021)**. In previous tests, the electrochemical method was used to calculate the corrosion rate, so the weight loss method will be adopted in this research.

2. EXPERIMENTAL PROCEDURE

This research carried out the practical aspect, starting with the preparation of DIN 1.0501 C35 carbon steel samples, from purchasing, cutting, cleaning, and polishing to the corrosion test. The aim is to use C35 carbon steel to test corrosion using the total immersion method and then calculate the corrosion rate using the weight loss equation. Each stage of these processes will be discussed in order.

2.1 Materials

The metal used in the ports of Basra to manufacture marine ship hulls was steel DIN 1.0501 C35, one of the most used metals in the construction of ship hulls. Although it does not resist corrosion well, it is used because it is cheap, can be formed, and can withstand external stresses **(Ali, 2019)**. The chemical composition of the steel was analyzed using an optical emission spectrometer, and a tensile test was conducted to ascertain its chemical properties, including maximum strength, yield strength, elongation and hardness. The specific values for these properties are detailed in **Tables 1 and 2.**

Table 1. Chemical composition of Carbon Steel Specimens.

Element %	C	Si	Mn	Ni	P	S	Cr	Mo	Fe
Standard **(ASTM D 1141–52, 1960**)	0.32-0.39	MAX 0.4	0.5-0.8	MAX 0.4	MAX 0.045	MAX 0.045	MAX 0.4	MAX 0.1	BALANCE
Measured	0.345	0.282	0.643	0.0611	0.02	0.0204	0.39	0.0321	BALANCE

Table 2. The results of testing the main mechanical properties.

Sample	Ultimate tensile Stress (UTS) N/mm^2	Yield Strength (YS) N/mm^2	Elongation %	Brinell (BHN)
Standard **(ASTM D 1141–52, 1960)**	650-1000	510	20	154
Cylinder (d=4mm)	520	275	18	119

The alloy composition primarily comprises iron, carbon, and other essential elements, including chromium, manganese, and sulfur **(Harrison et al., 1980)**. These elements, in precise proportions, collaboratively contribute to the alloy's overall mechanical and metallurgical properties **(Lippiatt et al., 2021)**. **Table 3** includes details about the materials used in this research. As shown below:

Table 3. The name of the item, the name of the company and the place where the experiment was conducted for the items used in this research.

Number	Item name	the supplier	Location
1	C35 carbon steel samples	Shandong Wufang Steel Group Company, Ltd.	Strength Laboratory, Mechanical Engineering Department, UOB.
2	Chemical composition test device (Spectrophotometer)	Niton™	Laboratory of the General Company for Engineering Inspection and Rehabilitation.
3	Tensile test device	Laryee Technology Co., Ltd	Strength Laboratory, Materials Engineering Department, UOT.
4	Hardness test device (BHN)	INNOVATEST	Strength Laboratory, Mechanical Engineering Department, UOB.
5	3 digits sensitive balance (GMA- 303)	Scale-Shop LLC.	Strength Laboratory, Mechanical Engineering Department, UOB.
6	TESCAN VEGA Scanning Electron Microscope	TESCAN	Nanotechnology and Advanced Materials Research Center laboratory, University of Technology.

2.2 Samples Preparation

DIN 1.0501 C35 steel was sourced from Shandong Wufang Steel Group Company, Ltd in China. The corrosion samples were precision-cut to meet the specified dimensions (50 mm × 50 mm × 5 mm), with ten samples—five allocated for static conditions and five for flow conditions, as shown in **Fig. 1** below.

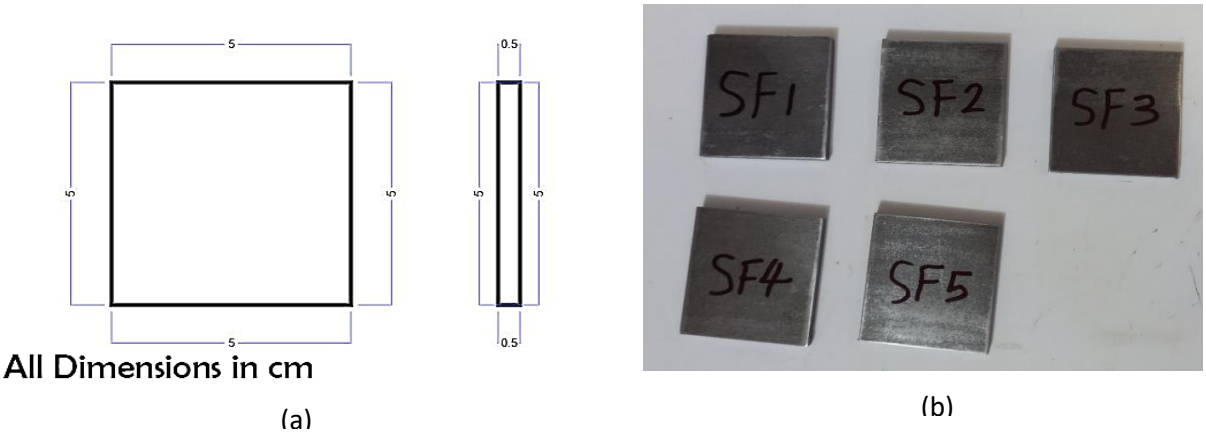

(a) (b)

Figure 1. (a) The dimensions of the corrosion sample, (b) the corrosion samples.

The preparation of samples involves two stages. The initial stage, employing a mechanical method, entails the removal of oxides and residual corrosion materials from the metal surface through polishing and grinding. This is achieved using sanding papers with varying degrees of roughness, including 120, 240, and 600 SiC sand grits. The sequence begins with rough papers, followed by fine papers and polishing, adhering to the procedures recommended by ASTM standards governing surface cleaning **(ASTM A380/A380M, 2017)**. The subsequent stage comprises washing the samples with distilled water, subsequently drying, cleaning the samples with the organic solvent acetone to eliminate suspended organic materials, and finally, rinsing them with distilled water before drying **(Zhang et al., 2021)**.

2.3 Solution Preparing

A sample of artificial seawater solution is prepared for use in the corrosion test of carbon steel. The laboratory-prepared artificial seawater adheres to the standard specification **(ASTM A380/A380M, 2017)**. The preparation involves adding 35 grams of sodium chloride salt to 1 liter of distilled water, ensuring a weight concentration of 3.5% sodium chloride. The accurate measurement of salt is carried out using a GMA-303 balance equipped with a precise three-digit sensor. The salt and distilled water are carefully weighed, as depicted in **Fig. 2** below.

(a) (b)

Figure 2. (a) Electronic balance GM Series (3 digits balance), (b) five liter bottles of distilled water.

Subsequently, the prepared solution is placed in a test pool equipped with a pump circulating water and air. This ensures all salts in the salty solution are wholly dissolved and prepared for corrosion **(Li et al., 2018)**.

2.4 Corrosion Test

The corrosion test process is carried out by immersing samples in a glass pool under the influence of artificial seawater under static and flowing seawater conditions. The corrosion of samples is examined with varying immersion times extending for more than a week at a constant temperature to determine the effect of immersion duration on the corrosion of C35 carbon steel. Upon sample preparation completion, the samples' initial weights (w1) are measured using the GMA-303 three-digit precision balance. Moreover, the dimensions of the samples are measured accurately to calculate the surface area of the samples. After weighing, a glass pool with dimensions (40 cm × 20 cm × 15 cm) is prepared and filled with artificial seawater previously prepared for the corrosion test. After that, a pump is placed to pump water to simulate the water flow process and measure the amount of erosion during the flow process. This involves using a water pump with a 1500 litres/hour flow rate. In addition, a DS18B20 temperature sensor is connected to monitor the temperature to keep the temperature parameter constant. The corrosion system as shown in **Fig. 3** below.

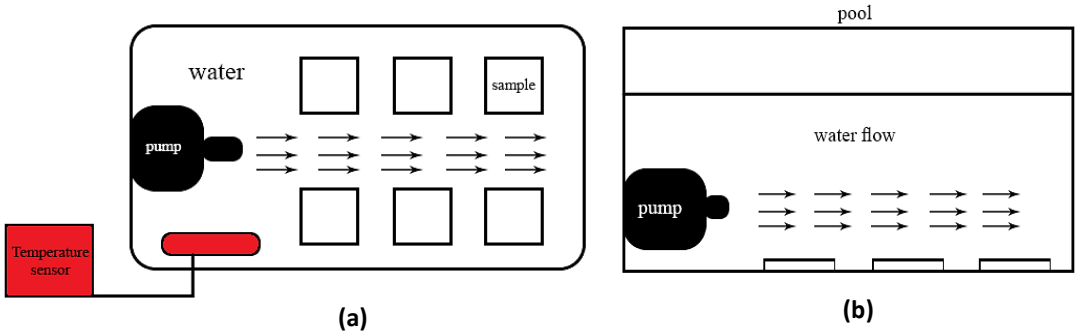

Figure 3. Total immersion system under flow conditions, where (a) top view of corrosion system, (b) front view of corrosion system.

Following the completion of the corrosion process on the samples, and with specific parameters changing while others remain constant, the samples are removed from the solution. Subsequently, the sample is weighed using a sensitive balance, and the new reading (w2) is recorded. After obtaining the readings, they are input into equations to calculate the corrosion rate. The equations for this purpose are as follows **(Al-Saadie, 2008)**:

$$\Delta wi = w1 - w2 \tag{3}$$

So that the corrosion rate can be determined using Eq. (4) **(Al-Saadie, 2008)**:

$$\mathrm{Cr} = \frac{K \times \Delta W}{\rho \times A \times t} \tag{4}$$

where k is constant is equal to 87.6 (to make the unit of corrosion rate in mm/y), ΔW is the weight loss (in mg), ρ is the carbon steel density is equal to 7.85 (in g/cm^3), A is the surface area (in cm^2), t is the exposure time to a corrosive environment (in hours).
The surface area can calculated using Eq. (5) **(Al-Saadie, 2008)**:

$$A = 2[(l \times b) + (b \times c) + (l \times c)] \quad (5)$$

where l is the length of the specimen, b is the width of the specimen, and c is the thickness of the specimen. So the surface area of the samples is obtained as 60 cm^2.

3. RESULTS AND DISCUSSION

After the conclusion of the immersion period for each sample, the samples were retrieved from the bottom of the pool. Subsequently, the samples were weighed after removing the oxide film from the metal surface. A comparison was then made between the corrosion products identified in the two test methods to understand and analyze the differences between the two methods in terms of their impact on the amount and rate of corrosion. Photographs of the samples extracted under static and flow conditions were captured (**Fig. 4**).

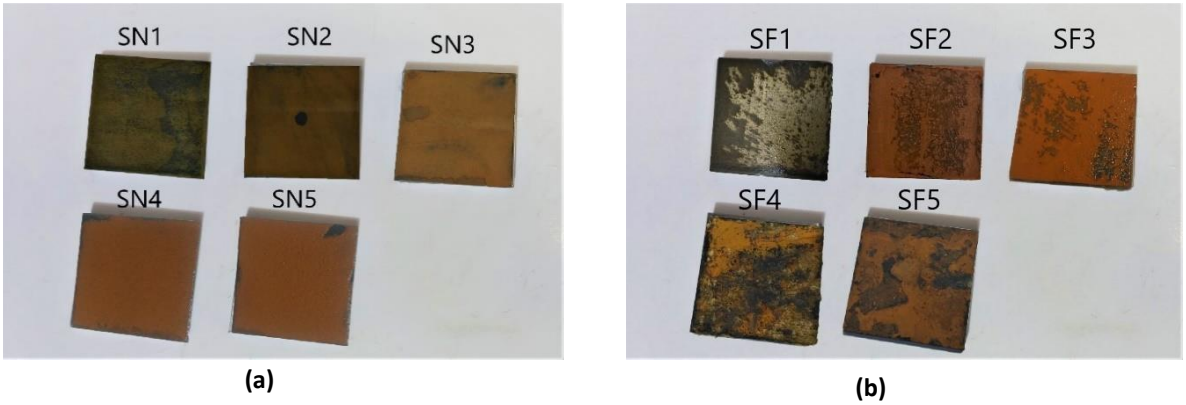

Figure 4. Pictures of corroded samples after removing it from the pool and before weighing the samples, under (a) Static conditions, (b) Flow conditions.

In **Fig. 4.a**, it is observable that a brown, chalky substance of iron oxide formed on the metal surface. The brown colour initially appeared slightly on the first sample SN1, and its density gradually increased with prolonged immersion time. The formation of this chalky brown layer is due to the formation of iron oxide, which depends mainly on contact and electrochemical interaction between the steel and salt water. The greater this contact and the period of immersion leads to the continuation of this reaction and the formation of this layer, increasing the density and color of this layer and making it clearer. Similar weight loss trends have been reported by **(Sang and Seung, 2017)**. Despite the abundance of this brown layer, its increased thickness, and the escalated loss of metal mass, it served as an insulating material. This protective layer prevents direct contact between the surface of C35 carbon steel and chloride ions in seawater, reducing the rate of electrochemical reactions responsible for the corrosion process, thereby reducing the chemical reaction between the metal and saltwater. The rate of corrosion decreased over time due to the gradual decrease in weight loss until it reached a stable situation. This is due to the increased thickness and effectiveness of the oxide layer in slowing down and decreasing the speed of the corrosion process. The rate of formation of the oxide layer is approximately equal to the rate at which it would be disrupted by salt water. And this is what happened with **(Jiangmin et al., 2021)**. The chalky material could be easily removed without leaving a trace, even on the last sample submerged for 168 hours.

In contrast, corrosion under flow conditions in **Fig. 4.b** was severe. The flow speed contributed to peeling the metal surface, revealing a fresh surface prone to new corrosion. This continuous corrosion subjected the metal surface to substantial weight loss, resulting in surface irregularities characterized by rises and depressions. The increased roughness is attributed to pit and groove corrosion after the second immersion day, and this is what happened with **(Yunze et al., 2020)**. Crusts at the bottom of the pool indicated the severity of corrosion and surface peeling due to the intense water flow. Despite this, the corrosion rate began to decrease under these conditions. It reached its highest rate on the second day but gradually decreased. This decrease in the corrosion rate is due to the formation of a protective passivation layer that slows down the formation of the electrochemical reaction. Although the rapid flow of seawater helps remove the outer oxide layer, the oxide layer can form again very quickly. Also, over time, an internal oxide layer will form that cannot be easily removed. Until it reaches a stage where the rate of loss of iron oxide resulting from the flow equals the rate of formation of iron oxide on the surface of C35 carbon steel, which leads to reaching a state closer to stability.

3.1 Weight-Loss Method

Before insertion into the pool, the samples underwent weighing, and the initial weight (W1) was recorded, as presented in **Table 3**. Following this, the samples were immersed in the pool for a specific duration. After the completion of this period, the samples were extracted from the pool's bottom, The sample was cleaned by spraying it with a commercial rust-dissolving chemical, WD-40. It is considered an effective solvent because it contains Isoparaffin and Aliphatic Hydrocarbons as main compounds in dissolving rust products. The sample is then cleaned with a brush and distilled water and the sample is then washed with acetone and then dried to remove corrosion products to ensure that the sample is thoroughly cleaned **(Abbass, 2011)**. Subsequently, the samples were dried and reweighed using a GMA-303 balance, and the second reading (W2) was recorded. The weight difference was then determined using Eq. (3), as follows: Data for sample SN3 is considered as an example for the calculation of the corrosion rate, such that:

$$\Delta wi = w1 - w2 = 95 - 94.967 = 0.033 \text{ g}$$

The corrosion rate of C35 carbon steel is obtained using Eq. (4), as:

$$\text{Cr} = \frac{K \times \Delta W}{\rho \times A \times t} = \frac{87.6 \times 33}{7.85 \times 60 \times 48} = 0.127866 \left(\frac{\text{mm}}{\text{year}}\right)$$

Table 4 contains the data for the samples and the deduced calculations for the weight loss process in static conditions when the temperature is constant. **Table 5** contains the deduced calculations for the weight loss process for the flow condition at a rate of 1500 L/hr when the temperature is constant.

It was noted that the data obtained revealed a significant increase in the corrosion rate under flow conditions compared to static conditions, recording an increase for the first 24-hour of the immersion period by 666%, for the 48-hour immersion period by 881.8%, and for the immersion period of 170 hour by 501%. The average increase for all immersion periods was 682.9%. This ratio was calculated using Eq. (6):

$$\% \text{ increase } = 100 \times \frac{(\text{final value} - \text{initial value})}{|\text{initial value}|} \quad (6)$$

Table 4. Corrosion rate data of static conditions.

Samples Name	W1 (g)	W2 (g)	ΔW (g)	CR(mm/year)	Hours
SN0	94.305	94.305	0	0	0
SN1	94.305	94.304	0.001	0.015499	12
SN2	94.908	94.887	0.021	0.162739	24
SN3	95	94.967	0.033	0.127866	48
SN4	94.781	94.702	0.079	0.122442	120
SN5	94.812	94.707	0.105	0.116242	168

Table 5. Corrosion rate data of flow conditions (1500 L/hr).

Samples Name	W1 (g)	W2 (g)	ΔW (g)	CR(mm/year)	Hours
SF0	94.65	94.65	0	0	0
SF1	94.65	94.58	0.07	1.084926	12
SF2	94.484	94.323	0.161	1.247665	24
SF3	95.037	94.713	0.324	1.255414	48
SF4	94.966	94.301	0.665	0.698766	177
SF5	94.891	93.715	1.176	0.65095541	336

This percentage signifies a remarkably high difference in results between the two scenarios. The inference drawn is that the flow environment proves highly corrosive and aggressive for the corrosion process of carbon steel metal **(Novák, 2007)**. Notably, the corrosion rate peaked on the first day under static conditions, while the highest levels were reached on the second day under inflow conditions. In both instances, the corrosion rate gradually declined until it stabilized after approximately a week of immersion. Utilizing the data from the corrosion test, charts depicting the corrosion rate and immersion time are generated based on the results obtained from the test, as shown in **Figs. 5** and **6**.

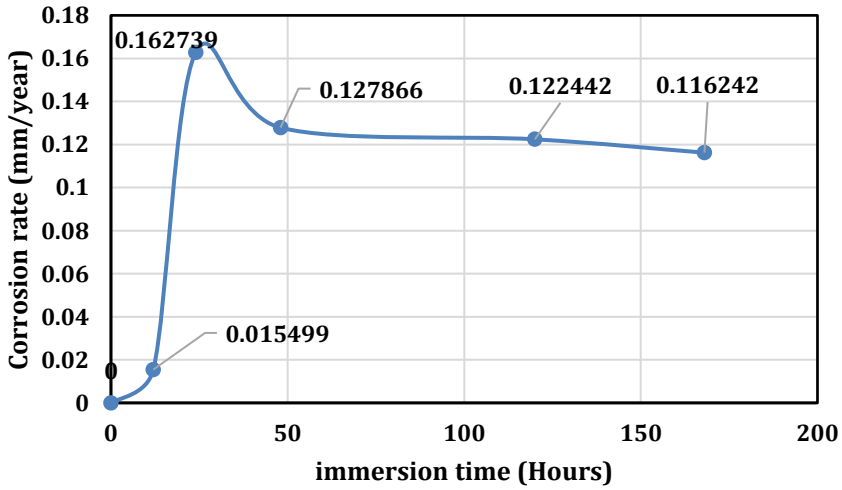

Figure 5. Corrosion rate with immersion time graph under static conditions.

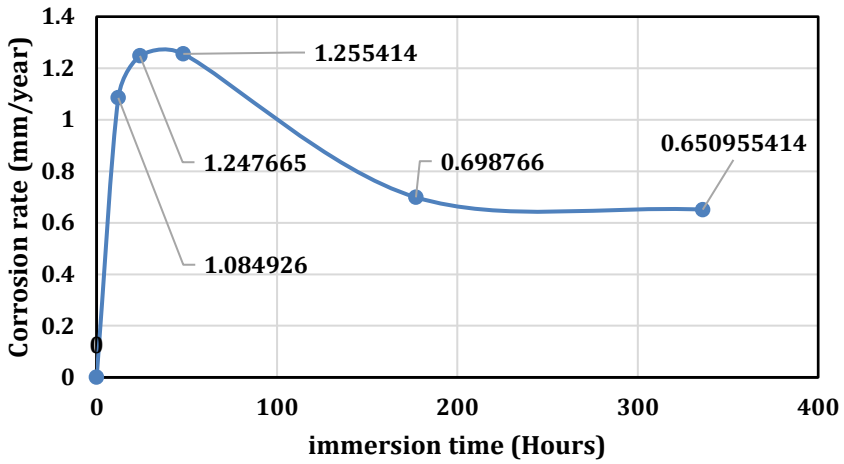

Figure 6. Corrosion rate with immersion time under flow conditions (1500 L/hr).

Based on the data in the two tables, two diagrams illustrating the relationship between weight loss and immersion time were drawn. It was observed that, despite the decrease in the corrosion rate, weight loss continued to increase over time. The increase in weight loss is attributed to the fact that weight loss increases with an increase in immersion time. This gradual increase can be observed in the charts **Figs. 7**and **8** below.

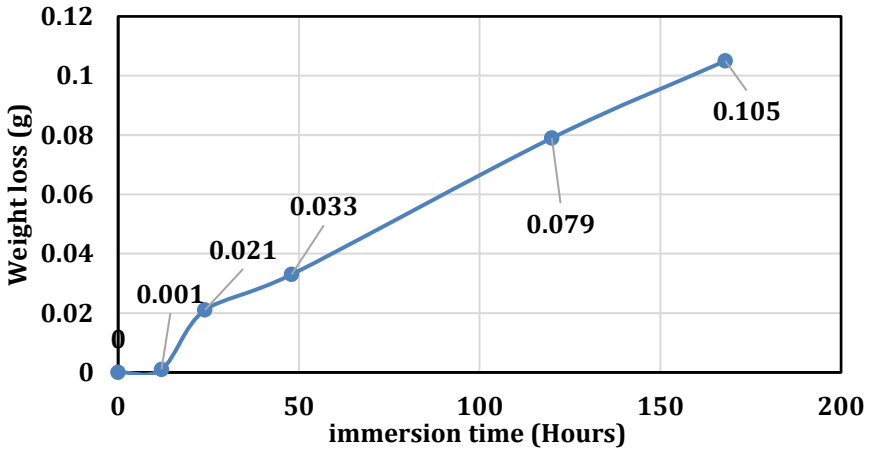

Figure 7. Weight loss with immersion time under static conditions.

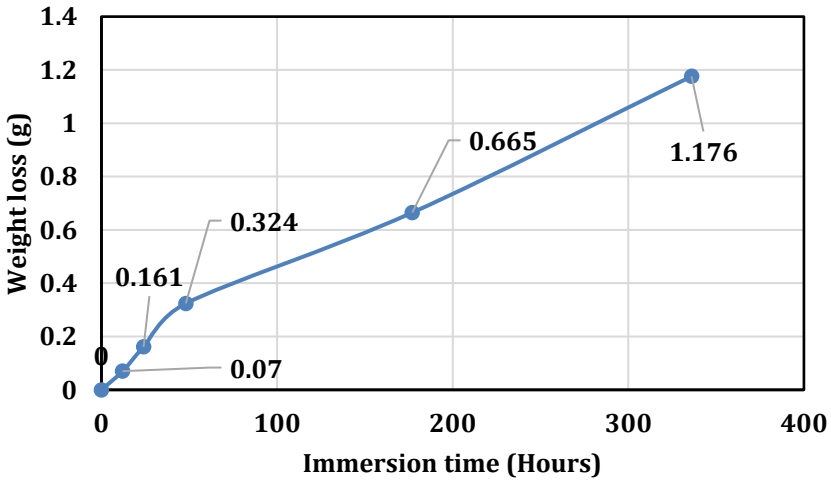

Figure 8. Weight loss with immersion time under flow conditions (1500 L/hr).

3.2 Prediction Corrosion Rate

A relationship that describes the system's behavior can be established using curve fitting. This equation closely matches the observed data, allowing interpolation and extrapolation **(Rao and Kuptsov, 2015)**. Microsoft Excel obtains curve fitting, such as LINEST and TREND, for linear regression and polynomial curve fitting **(Quirk, 2016)**. The Linear Least Square method **(Ji et al., 2015)** is used for the system such as in Eq. (7):

$$\bar{CR} = a0 + a1\bar{t} \tag{7}$$

where $\bar{CR}$ is the corrosion rate in (mm/year), $\bar{t}$ is the immersion time in (hours) and *a0, a1* are constants can be evaluated as the following:

$$a0 = \frac{\sum_{i=1}^{n} t^2 \sum_{i=1}^{n} CR - \sum_{i=1}^{n} CRt \sum_{i=1}^{n} t}{n\sum_{i=1}^{n} t^2 - (\sum_{i=1}^{n} t)^2} \tag{8}$$

$$a1 = \frac{n\sum_{i=1}^{n} CRt - \sum_{i=1}^{n} CR \sum_{i=1}^{n} t}{n\sum_{i=1}^{n} t^2 - (\sum_{i=1}^{n} t)^2} \tag{9}$$

where CR is the corrosion rate in (mm/year), t is the immersion time in (hours) and n is the number of input data. The special prediction corrosion rate for the conditions static and flow at a rate of 1500 L/hr, are:

$$\Delta W_{(\text{Static conditions})} = 0.0006\text{t} + 0.0003 \tag{10}$$

$$\Delta W_{(\text{Flow conditions})} = 0.0034\text{t} + 0.0655 \tag{11}$$

The estimation results obtained from the prediction equations for the static and flow conditions are included. As shown in **Table 6** below:

Table 6. Predictive data from the prediction relationship for the static and flow conditions.

Samples Name	t (hr)	ΔW (static)	CR(static)	ΔW (flow)	CR(flow)
1	5	0.0033	0.122752	0.0825	3.06879
2	30	0.0183	0.113452	0.1675	1.038429
3	50	0.0303	0.112708	0.2355	0.876
4	75	0.0453	0.112336	0.3205	0.794786
5	100	0.0603	0.11215	0.4055	0.754178
6	150	0.0903	0.111964	0.5755	0.713571
7	200	0.1203	0.111871	0.7455	0.693268
8	400	0.2403	0.111732	1.4255	0.662812
9	700	0.4203	0.111672	2.4455	0.64976
10	1000	0.6003	0.111648	3.4655	0.644539

In which the weight loss value is estimated for points in the chart at any unknown data point, and that shown in the charts of curve fitting for static and flow conditions in **Fig. 9** and **10**.

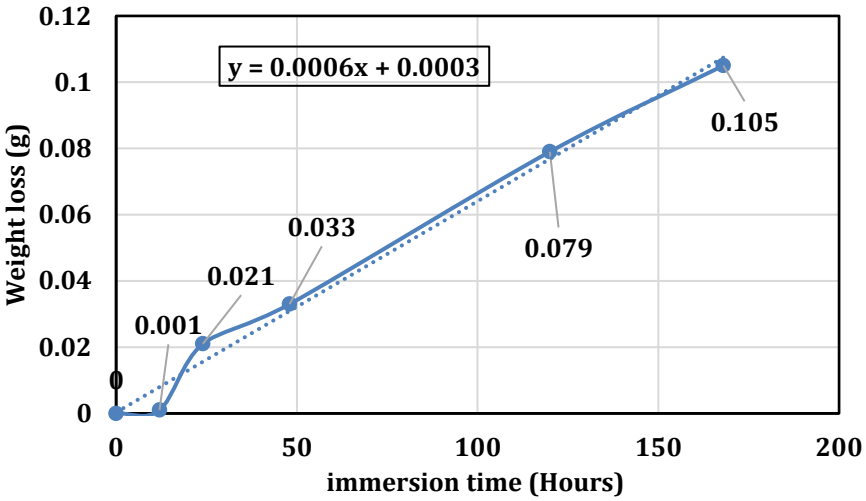

Figure 9. Weight loss with immersion time using Least squares curve fitting graph for static conditions.

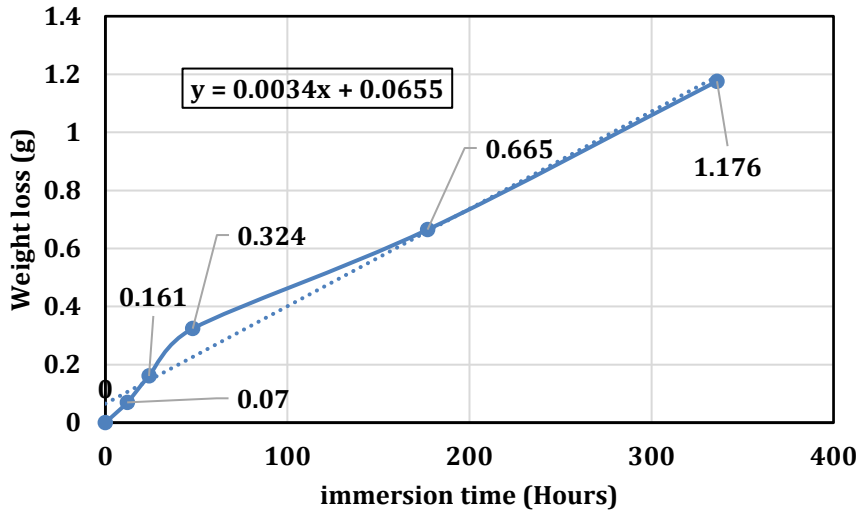

Figure 10. Weight loss with immersion time using Least squares curve fitting for flow conditions (1500 l/hr).

3.3 SEM Analysis

Scanning Electron Microscope (SEM) was used to determine samples' surface topography after the metal failed a corrosion test. The metals at risk of failure were sent to the Nanotechnology and Advanced Materials Research Center laboratory located in the College of Engineering at the University of Technology, where the samples were examined and photographed using SEM. **Fig. 11** shows the scanning electron microscope (SEM) results for corroded samples after 170 hours of immersion with different zoom. The results show that the surface morphology of the static condition sample is substantially different from the surface morphology of the flow condition sample. It is observed from **Fig. 11** (**a** and **b**) that the corrosion in the static condition occurred with a thick layer of corrosion because the corrosion occurred in a static environment, and the oxide layer maintained itself and increased in thickness as the corrosion continued. Pitting corrosion, groove corrosion, and cracks were observed in some areas but not others, indicating that local corrosion occurred

on the surface of the carbon steel sample. It was noted from **Fig. 11** (**c** and **d**) that the corrosion in the flowing condition occurred with a more aggressive and worse layer than in the static state. Pit and groove corrosion was observed in a prominent and significant manner due to the aggressive environment resulting from the flow. Although corrosion is spread randomly on the surface of the metal, the corrosion tends to be regular because pit and groove corrosion is spread over the entire surface.

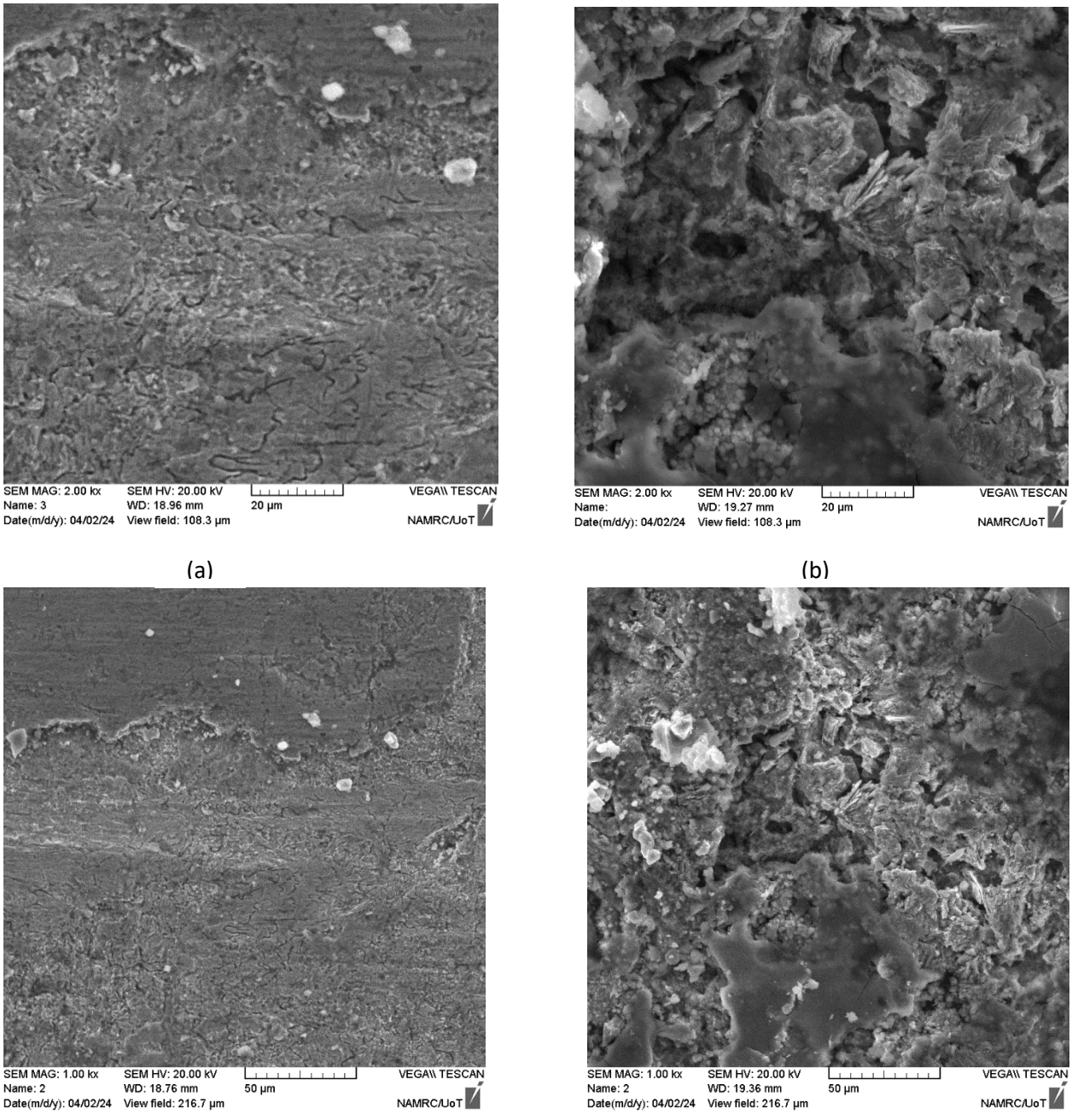

Figure 11. SEM photograph of C35 Carbon steel after 170 hours of immersion with different zoom (a) SN5 (static condition sample) with zoom 2000X, (b) SN5 (static condition sample) with zoom 1000X, (c) SN4 (flow condition sample) with zoom 2000X, (d) SN4 (flow condition sample) with zoom 1000X.

4. CONCLUSIONS

The following conclusions were drawn from this research. With an increase in the flow rate, there was a corresponding increase in the corrosion rate, with the corrosion rate doubling for samples subjected to flow conditions compared to those in static conditions. The corrosion rate experienced a notable increment of approximately 682.9% in the flow conditions when contrasted with the static conditions. In static conditions, corrosion was not severe, whereas in flow conditions, corrosion was pronounced, resulting in the formation of pitting and groove corrosion on the metal surface. The corrosion rate exhibited a significant surge in the initial 24 hours, followed by a gradual decrease with prolonged immersion time. Initially, the corrosion process was rapid, but after 24 hours of immersion, the weight loss decelerated. A scanning electron microscope (SEM) examination revealed that the flow environment was aggressive for carbon steel. It was much more severe, and the pits and grooves were more significant than the static condition.

NOMENCLATURE

Symbol	Description	Symbol	Description
A	Surface area, cm^2	K	Constant, 87.6
a0	Constant	l	Length, cm
a1	Constant	t	Time, h
b	Width, cm	ΔW	Weight loss, mg
c	Thickness, cm	ρ	Density, g/cm^3
Cr	Corrosion rate, mm/year		

ACKNOWLEDGMENTS

The authors are grateful to the crew of ship port engineers in Basra for their cooperation. Full appreciation to the Shandong Wufang Steel Group Co., Ltd in China for the accuracy of production. The authors thank the Mechanical Engineering Laboratory staff for their cooperation and facilitation.

Credit Authorship Contribution Statement

Abdul-Hamied Ayad: Writing –original draft, Validation, Methodology.
Abdullah Dhayea: Review & editing, Validation, Proofreading.

Declaration of Competing Interest

The authors declare that they have no known competing financial interests or personal relationships that could have appeared to influence the work reported in this paper.

REFERENCES

Abbass, M., Ahmed, M., and Hazem, M., 2011. Effect of the heat treatments on corrosion and erosion-corrosion for carbon steel. *Engineering and Technology Journal*, *29*(13), pp. 2706-2722. https://doi.org/10.30684/etj.29.13.10

Abd, R., and Hammadi, N., 2022. estimating pitting corrosion depth and density on carbon steel (C-4130) using artificial neural networks. *Journal of Engineering*, *28*(5), pp. 11–24. https://doi.org/10.31026/j.eng.2022.05.02

Ahmed, S., and Makki, H., 2019. Corrosion rate optimization of mild-steel under different cooling tower working parameters using taguchi design. *Journal of Engineering*, *26*(1), pp. 174–185. https://doi.org/10.31026/j.eng.2020.01.13

Ali, N., Putra, T., Iskandar, V., and Thalib, S., 2019. corrosion rate of low carbon steel for construction materials in various NaCl concentrations. *Materials Science and Engineering,* 536(1), P. 012015. https://doi.org/10.1088/1757-899X/536/1/012015

Alsaadi, H., 2015. Corrosion study of the injection equipments in water in Al-Ahdeb Wells - Iraq. *Journal of Engineering*, *21*(1), pp. 15–28. https://doi.org/10.31026/j.eng.2015.01.02

Al-Saadie, K., 2008. The Effect of linear alkyl benzene sulfonate on corrosion of aluminum, zinc and lead in 1M HCl. *Iraqi National Journal of Chemistry*, 8(29), pp. 76-86.

Andrade, C., and Alonso, C., 1996. Corrosion rate monitoring in the laboratory and on-site. *Construction and building materials*, *10*(5), pp. 315-328. https://doi.org/10.1016/0950-0618(95)00044-5

ASTM D 1141–52, 1960. Standard specifications for substitute ocean water.

ASTM A380/A380M, 2017. Standard practice for cleaning, descaling, and passivation of stainless steel parts, equipment, and systems.

Bringas, J.E., 2004. Hand Book of Comparative World Steel Standard, 3rd edition. Library of Congress Cataloging-in-Publication Data. USA. ISBN 0-8031-3042-2.

Choe, S., and Lee, S., 2017. Effect of flow rate on electrochemical characteristics of marine material under seawater environment. *Ocean Engineering*, 141, pp. 18-24. https://doi.org/10.1016/j.oceaneng.2017.05.035

Cox, G., and Roetheli, B., 1931. Effect of oxygen concentration on corrosion rates of steel and composition of corrosion products formed in oxygenated water. *Industrial and Engineering Chemistry*, *23*(9), pp. 1012-1016. https://doi.org/10.1021/ie50261a011

Doos, Q., and Farhan, R., 2014. Study of the friction stir welding for A516 low carbon steel. *Journal of Engineering*, *20*(1), pp. 132–150. https://doi.org/10.31026/j.eng.2014.01.10

Dwivedi, D., Lepková, K., and Becker, T., 2017. Carbon steel corrosion: a review of key surface properties and characterization methods. *RSC advances*, 7(8), pp. 4580-4610. https://doi.org/10.1039/C6RA25094G

Harrison, P., Waters, R., and Taylor, F., 1980. A broad spectrum artificial sea water medium for coastal and open ocean phytoplankton 1. *Journal of phycology*, *16*(1), pp. 28-35. https://doi.org/10.1111/j.0022-3646.1980.00028.x

Hasan, B., Al-habubi, N., and Hussien, S., 2016. Galvanic corrosion of carbon steel -stainless steel couple in sulfuric acid under flow conditions. *Journal of Engineering*, *22*(8), pp. 158–174. https://doi.org/10.31026/j.eng.2016.08.10

Hiekata, K., and Grau, M., 2015. Shipbuilding. *Concurrent Engineering in the 21st Century: Foundations, Developments and Challenges*. Springer Cham. https://doi.org/10.1007/978-3-319-13776-6_23

Ji, J., Zhang, C., Kodikara, J., and Yang, S., 2015. Prediction of stress concentration factor of corrosion pits on buried pipes by least squares support vector machine. *Engineering Failure Analysis*, *55*, pp. 131-138. https://doi.org/10.1016/j.engfailanal.2015.05.010

Kaouka, A., Allaf, H., Keddam, M., and Alaoui, O., 2022. Evaluating the corrosion behaviour of borided carbon steel C35. *Materials Research*, *25*, e20200591. https://doi.org/10.1590/1980-5373-MR-2020-0591

Li, Y., Zhao, X., and Raman, R., 2018. Mechanical properties of seawater and sea sand concrete-filled FRP tubes in artificial seawater. *Construction and building materials*, 191, pp. 977-993. https://doi.org/10.1016/j.conbuildmat.2018.10.059

Lippiatt, K., Bell, S., Ong, T., East, C., McAuley, D., Will, G., and Steinberg, T., 2021. An improved technique for molten salt corrosion sample preparation. *Solar Energy Materials and Solar Cells*, 226, P. 111057. https://doi.org/10.1016/j.solmat.2021.111057

Machuca, L., Jeffrey, R., Bailey, S., Gubner, R., Watkin, E., Ginige, M., Kaksonen, A., and Heidersbach, K., 2014. Filtration–UV irradiation as an option for mitigating the risk of microbiologically influenced corrosion of subsea construction alloys in seawater. *Corrosion Science*, *79*, pp. 89-99. https://doi.org/10.1016/j.corsci.2013.10.030

Majbor, K., Alias, Q., Tobia, W., and Hamed, M., 2017. Cathodic protection design algorithms for refineries aboveground storage tanks. *Journal of Engineering*, *23*(12), pp. 82–95. https://doi.org/10.31026/j.eng.2017.12.06

McCafferty, E., 2010. Introduction to corrosion science. *Springer Science and Business Media*. https://doi.org/10.1007/978-1-4419-0455-3

Muhammad, M., Mohammed, B., Ahmed, F., and Al Numan, B., 2021. Critical evaluation for grading and fineness modulus of concrete sands used in Sulaymaniyah city-Iraq. *Journal of Engineering*, *27*(10), pp. 34–49. https://doi.org/10.31026/j.eng.2021.10.03

Nader, A., and Shather, S., 2022. Effect of abrasive water jet (AWJ) parameters on materials removal rate for low carbon steel. *Engineering and Technology Journal*, *40*(06), pp. 885-891. https://doi.org/10.30684/etj.v40i6.2123

Novák, P., 2007. Environmental deterioration of metals. *Environmental Deterioration of Materials*; Escrig, F., Managing Ed.; WIT Press: Boston, pp. 27-71. https://doi.org/10.1016/C2010-0-66227-4

Quirk, J.T., 2016. Excel 2016 for business statistics. Springer Cham, Springer International Publishing Switzerland. https://doi.org/10.1007/978-3-319-38959-2

Rao, D., and Kuptsov, V., 2015. Effective use of magnetization data in the design of electric machines with overfluxed regions. *IEEE Transactions on Magnetics*, *51*(7), pp. 1-9. https://doi.org/10.1109/TMAG.2015.2397398

Rashid, K., Shakor, Z., and Ahmed, A., 2017. Modelling and optimization of corrosion inhibition of mild steel in phosphoric acid by red pomegranate peels aqueous extract. *Journal of Engineering*, *23*(11), pp. 25–42. https://doi.org/10.31026/j.eng.2017.11.03

Salman, E., 2018. Experimental investigation of the electro co-deposition of (Zinc-Nickel) alloy. *Journal of Engineering*, *24*(2), pp. 46–61. https://doi.org/10.31026/j.eng.2018.02.04

Saravanan, M., and Kumar, D., 2021. A review on navy ship parts by advanced composite material. *Materials Today: Proceedings*, *45*, pp. 6072-6077. https://doi.org/10.1016/j.matpr.2020.10.074

Shakir, I., Alsamurraee, A., and Saleh, S., 2018. Pitting corrosion behavior of 304 SS and 316 SS alloys in aqueous chloride and bromide solutions. *Journal of Engineering*, *24*(1), pp. 53–69. https://doi.org/10.31026/j.eng.2018.01.04

Shreir, L., 2013. Corrosion: metal/environment reactions. *Newnes*. https://doi.org/10.1016/C2013-0-04015-7

Tamura, H., 2008. The role of rusts in corrosion and corrosion protection of iron and steel. *Corrosion Science*, *50*(7), pp. 1872-1883. https://doi.org/10.1016/j.corsci.2008.03.008

Xia, J., Li, Z., Jiang, J., Wang, X., and Zhang, X., 2021. Effect of flow rates on erosion corrosion behavior of hull steel in real seawater. *International Journal of Electrochemical Science*, 16(5), P. 210532. https://doi.org/10.20964/2021.05.60

Xu, Y., Liu, L., Xu, C., Wang, X., Tan, M. Y., and Huang, Y., 2020. Electrochemical characteristics of the dynamic progression of erosion-corrosion under different flow conditions and their effects on corrosion rate calculation. *Journal of Solid State Electrochemistry*, 24, pp. 2511-2524. https://doi.org/10.1007/s10008-020-04795-9

Zhang, H., Yan, L., Zhu, Y., Ai, F., Li, H., Li, Y., and Jiang, Z., 2021. The effect of immersion corrosion time on electrochemical corrosion behavior and the corrosion mechanism of EH47 ship steel in seawater. *Metals*, *11*(8), P. 1317. https://doi.org/10.3390/met11081317

تقييم تأثير الظروف الساكنة والمتدفقة على سلوك تآكل بدن السفن البحرية

عبدالحميد أياد عبدالحميد*، عبدالله ضايع عاصي

قسم الهندسة الميكانيكية، كلية الهندسة، جامعة بغداد، بغداد، العراق

الخلاصة

تم دراسة سلوك مقاومة تآكل هياكل السفن البحرية في ظل الظروف الساكنة والمتدفقة، من خلال فحص وتحليل معادن ألواح هياكل السفن البحرية كيميائياً وميكانيكياً، وتبين أن الفولاذ الكربوني نوع DIN 1.0501 C35 يستخدم في بناء هياكل السفن في ميناء البصرة في العراق. تم إجراء اختبار مقاومة التآكل لهذا المعدن في مياه البحر المحضرة مخبرياً تحت ظروف ثابتة ومتدفقة بمعدل تدفق 1500 لتر/ساعة وأوقات غمر مختلفة (12، 24، 48، 120، 168، 336) ساعة. تم الحفاظ على درجة الحرارة ثابتة عند 30 درجة مئوية، وتم الحفاظ على تركيز ملح ثابت (3.5% كلوريد الصوديوم). تم حساب معدل التآكل للفولاذ الكربوني C35 باستخدام طريقة فقدان الوزن وهي طريقة فعالة لحساب معدل تآكل الفولاذ الكربوني. تم فحص العينات باستعمال المجهر الإلكتروني الماسح (SEM) من اجل تحليل التاكل. استنتج من هذا البحث إلى أن زيادة معدل التدفق أدى إلى ارتفاع معدل التآكل، حيث تضاعف معدل التآكل مقارنة بالعينات تحت الظروف الساكنة. أظهر معدل التآكل زيادة كبيرة خلال الـ 24 ساعة الأولى، يليه انخفاض تدريجي مع زيادة وقت الغمر، حيث شهد معدل التآكل زيادة بنسبة 682.9٪. وكانت سرعة التآكل سريعة في البداية، لكن فقدان الوزن تباطأ بعد 24 ساعة من الغمر. لوحظ من فحص المجهر الإلكتروني الماسح (SEM) ان بيئة التدفق هي بيئة عدوانية للفولاذ الكربوني، فلقد كان اشد بكثير وكانت النقرات والاخاديد اكبر حجما مقارنة مع حالة السكون.

الكلمات المفتاحية: تاكل السفن، تاكل الفولاذ، مياه البحر، C35 فولاذ كاربوني، طريقة فقدان الوزن.